Nonadiabatic coupling vectors for excited states within time-dependent density functional theory in the Tamm–Dancoff approximation and beyond

Ivano Tavernelli, Basile F. E. Curchod, Andrey Laktionov, and Ursula Rothlisberger

Citation: The Journal of Chemical Physics **133**, 194104 (2010); doi: 10.1063/1.3503765
View online: http://dx.doi.org/10.1063/1.3503765
View Table of Contents: http://scitation.aip.org/content/aip/journal/jcp/133/19?ver=pdfcov
Published by the AIP Publishing

Nonadiabatic coupling vectors for excited states within time-dependent density functional theory in the Tamm–Dancoff approximation and beyond

Ivano Tavernelli,[a] Basile F. E. Curchod, Andrey Laktionov, and Ursula Rothlisberger
Laboratory of Computational Chemistry and Biochemistry, Ecole Polytechnique Fédérale de Lausanne, Lausanne CH-1015, Switzerland

(Received 9 July 2010; accepted 29 September 2010; published online 16 November 2010)

Recently, we have proposed a scheme for the calculation of nonadiabatic couplings and nonadiabatic coupling vectors within linear response time-dependent density functional theory using a set of auxiliary many-electron wavefunctions [I. Tavernelli, E. Tapavicza, and U. Rothlisberger, J. Chem. Phys. **130**, 124107 (2009)]. As demonstrated in a later work [I. Tavernelli, B. F. E. Curchod, and U. Rothlisberger, J. Chem. Phys. **131**, 196101 (2009)], this approach is rigorous in the case of the calculation of nonadiabatic couplings between the ground state and any excited state. In this work, we extend this formalism to the case of coupling between pairs of singly excited states with the same spin multiplicity. After proving the correctness of our formalism using the electronic oscillator approach by Mukamel and co-workers [S. Tretiak and S. Mukamel, Chem. Rev. (Washington, D.C.) **102**, 3171 (2002)], we tested the method on a model system, namely, protonated formaldimine, for which we computed S_1/S_2 nonadiabatic coupling vectors and compared them with results from high level (MR-CISD) electronic structure calculations. © *2010 American Institute of Physics*. [doi:10.1063/1.3503765]

I. INTRODUCTION

Linear response time-dependent density functional theory (LR-TDDFT)[1,2] has become one of the most widely used numerical approaches for the calculation of vertical excitation energies[1,3,4] and excited state properties[5,6] of medium to large size molecular systems in gas and condensed phases.[7,8] Despite its widespread usage and the number of successful applications in different research areas in physics, chemistry, and biology,[9–14] there are important failures of the method related, in particular, to the description of charge transfer (CT) states,[15] $\pi \rightarrow \pi^*$ transitions in large aromatic molecules,[16,17] hyperpolarizabilities,[18] ionic singlet excitations,[19] and for nearly degenerate states.[20,21] Recently, excited state LR-TDDFT energy gradients have also become available,[6,22] which allow for an efficient calculation of *ab initio* forces on the nuclei. The combination of LR-TDDFT energies and nuclear forces finally makes the development of an efficient *ab initio* molecular dynamics (AIMD) scheme for the study of photophysical and photochemical processes possible.[12,13] Originally formulated within the so-called Born–Oppenheimer (BO) approximation, AIMD in excited states often requires the inclusion of nonadiabatic corrections to deal with nuclear quantum effects in regions of strong nonadiabatic coupling (avoided crossings).[10,12,23–28]

Nonadiabatic couplings (NACs) describe the dynamical interaction between the electronic and the nuclear motion in regions of configurational space where the potential energy surfaces cross or nearly cross. They give a measure of the deviation of the exact full quantum (electrons and nuclei) dynamics from the adiabatic BO approximation. The knowledge of the NACs is therefore crucial for the development of an AIMD approach that is able to describe excited state dynamics of a large class of chemical and biological processes that occur in the nonadiabatic regime. In particular, for reactions that take place at the intersection of two or more potential energy surfaces (PESs), where NACs become large and divergent, the inclusion of nonadiabatic effects is essential for a correct description of the dynamics. It is however important to mention that, despite the *in principle* exact nature of the LR-TDDFT excited state energies and NACs, in practice their calculation require the use of approximated DFT functionals and LR-TDDFT kernels. These approximations introduce inevitably some limitations in the use of TDDFT-based nonadiabatic AIMD, which are related to the LR-TDDFT failures listen above and that in some cases may lead to a wrong topology of the PESs near the regions of strong coupling.[13,21] On the other hand, the coupling between excited states may not suffer from the shortcomings observed, in some cases, for the S_0/S_1 crossings (singlet instabilities,[20] weak coupling, and wrong dimensionality of the crossing seam),[13,21] but due to the fact that excited states are treated on equal footing within LR-TDDFT (when no CT or Rydberg states are considered) we expect that some properties might be more accurate.

The main issue regarding the computation of the NACs using LR-TDDFT lies in the intrinsic difficulty to compute expectation values and transition matrix elements of observables, which are not simple functionals of the electronic density or its corresponding Kohn–Sham orbitals. Among those are the nonadiabatic coupling matrix elements and vectors (NACVs), whose calculation requires the knowledge of the many-electron wavefunctions of the two states involved in the coupling. Nonetheless, several approaches for the calculation of the NACs and NACVs in LR-TDDFT have been

[a]Electronic mail: ivano.tavernelli@epfl.ch.

recently developed. All these methods strictly apply to the linear case in which one of the two states involved in the coupling is the ground state. The first closed expression for the calculation of the NACs within LR-TDDFT was given by Chernyak and Mukamel[29] using a density-matrix formulation of LR-TDDFT. This work was followed by the interesting development of Baer[30] based on the calculation of the NACVs between ground and excited states using real-time propagation TDDFT. Later, Tapavicza *et al.*[27,31,32] and Hu *et al.*[33] independently suggested an alternative formulation built on Casida's equations,[1] which provides a very efficient way for the computation of NACs and NACVs that can easily be applied to large molecular systems. Despite their common theoretical framework, it was not evident at first glance if these two theories were footed on the same approximations, especially in view of the fact that in one case[27,31] a reconstruction of an auxiliary many-electron wavefunction for excited states was introduced. Recently,[34] we showed that the NACVs obtained using the auxiliary many-electron wavefunctions[32] are indeed identical to the ones of Ref. 33.

In this paper, we will first prove the correctness and then assess the quality of the NACVs computed for a pair of excited states using the approach based on the auxiliary many-electron wavefunctions.[31,34] The proof of the validity of this approach was originally formulated only for the case of NACVs between the ground state and an excited state. Using the "effective multilevel system" (EMS) proposed by Tretiak and co-workers,[35,36] we show that the NACVs computed using the auxiliary many-electron wavefunctions[31,34] represent a good approximation, which becomes exact when the Tamm–Dancoff approximation (TDA) to the LR-TDDFT equations is invoked.

In Sec. II, we review the basic TDDFT equations beyond first-order in the density perturbation.[35] The second-order TDDFT density-density response function is briefly introduced in Sec. III, where we also derive expressions for the calculation of matrix elements beyond linear response. In Sec. IV, we compare EMS second-order matrix elements with the corresponding quantities obtained from LR-TDDFT in the auxiliary many-electron wavefunctions formulation,[31,34] in particular in the TDA. A comparison of the NACVs computed within LR-TDDFT and the wavefunction-based approach MR-CISD for the protonated formaldimine test system is given in Sec. V. Section VI summarizes and concludes.

II. DENSITY MATRIX EQUATION OF MOTIONS FOR TDDFT

The phase space Hamilton–Liouville equations of motion for the density ρ are given by

$$i\frac{d\rho}{dt} = \{H_T, \rho\}, \tag{1}$$

where $\{\cdots\}$ are the Poisson brackets and H_T is the total Hamiltonian[35,37]

$$H_T[\rho] = E^0_{\mathrm{KS}}[\rho] + \int d\boldsymbol{r} U_{\mathrm{pert}}(\boldsymbol{r},t)\rho(\boldsymbol{r},t). \tag{2}$$

The density perturbation $\delta\rho(\boldsymbol{r},t) = \rho(\boldsymbol{r},t) - \rho(\boldsymbol{r})$ obeys the time-dependent differential equation

$$i\frac{d\,\delta\rho(\boldsymbol{r},t)}{dt} = [F[\rho],\rho] + [U_{\mathrm{pert}},\rho], \tag{3}$$

where the outer square brackets denote the commutator between the two operators, and $F[\rho]$ is the Kohn–Sham (KS) operator defined by the exchange-correlation functional $V_{xc}[\rho]$.

In order to compute linear and nonlinear response functions, we expand E_{KS} as a Taylor series to third order in $\delta\rho$ around the equilibrium density ρ_0,[36,38]

$$E_{\mathrm{KS}}[\rho] = E^0_{\mathrm{KS}}[\rho] + V'[\rho] + V''[\rho] + V'''[\rho], \tag{4}$$

with

$$V'[\delta\rho] = \int d\boldsymbol{r}' \left(\frac{1}{|\boldsymbol{r}-\boldsymbol{r}'|} + f_{xc}[\rho_0](\boldsymbol{r},\boldsymbol{r}') \right) \delta\rho(\boldsymbol{r}',t), \tag{5}$$

$$V''[\delta\rho,\delta\rho] = \frac{1}{2!}\int d\boldsymbol{r}' \int d\boldsymbol{r}'' g_{xc}[\rho_0](\boldsymbol{r},\boldsymbol{r}',\boldsymbol{r}'')\,\delta\rho(\boldsymbol{r}',t)\,\delta\rho(\boldsymbol{r}'',t), \tag{6}$$

$$V'''[\delta\rho,\delta\rho,\delta\rho] = \frac{1}{3!}\int d\boldsymbol{r}' \int d\boldsymbol{r}'' \int d\boldsymbol{r}''' h_{xc}[\rho_0](\boldsymbol{r},\boldsymbol{r}',\boldsymbol{r}'',\boldsymbol{r}''') \times \delta\rho(\boldsymbol{r}',t)\,\delta\rho(\boldsymbol{r}'',t)\,\delta\rho(\boldsymbol{r}''',t), \tag{7}$$

and

$$f_{xc}[\rho](\boldsymbol{r},\boldsymbol{r}') = \left.\frac{\delta V_{xc}[\rho](\boldsymbol{r})}{\delta\rho(\boldsymbol{r}')}\right|_{\rho_0}, \tag{8}$$

$$g_{xc}[\rho](\boldsymbol{r},\boldsymbol{r}',\boldsymbol{r}'') = \left.\frac{\delta^2 V_{xc}[\rho](\boldsymbol{r})}{\delta\rho(\boldsymbol{r}')\,\delta\rho(\boldsymbol{r}'')}\right|_{\rho_0}, \tag{9}$$

$$h_{xc}[\rho](\boldsymbol{r},\boldsymbol{r}',\boldsymbol{r}'',\boldsymbol{r}''') = \left.\frac{\delta^3 V_{xc}[\rho](\boldsymbol{r})}{\delta\rho(\boldsymbol{r}')\,\delta\rho(\boldsymbol{r}'')\,\delta\rho(\boldsymbol{r}''')}\right|_{\rho_0}, \tag{10}$$

in the adiabatic approximation.

When expanded in Kohn–Sham orbitals, the density variation $\delta\rho$ can be divided in two components,[36]

$$\delta\rho(\boldsymbol{r},t) = \xi(\boldsymbol{r},t) + T(\xi(\boldsymbol{r},t)), \tag{11}$$

where $\xi(\boldsymbol{r},t)$ represents the particle-hole and hole-particle (interband) and $T(\xi(\boldsymbol{r},t))$ the particle-particle and hole-hole (intraband) parts. Only the interband elements are independent and the intraband elements can be expressed as a function of $\xi(\boldsymbol{r},t)$,

$$T(\xi(\boldsymbol{r},t)) = (I - 2\rho_0)(\xi^2 + \xi^4 + 2\xi^6\cdots). \tag{12}$$

Using the interband projector of the density perturbation $\delta\rho(t)$,

$$\xi(\mathbf{r},t)=[[\delta\rho(\mathbf{r},t),\rho_0(\mathbf{r})],\rho_0(\mathbf{r})], \tag{13}$$

one obtains the nonlinear TDDFT equation in the interband subspace

$$i\frac{\partial\xi}{\partial t}-\mathcal{L}\xi=\mathcal{R}(\xi)-[U_{\text{ext}},\rho_0], \tag{14}$$

where the linear TDDFT Liouville operator is given by

$$\mathcal{L}\xi=[F(\rho_0),\xi]+[V'(\xi),\rho_0] \tag{15}$$

and[36]

$$\begin{aligned}\mathcal{R}(\xi)=&-[U_{\text{pert}},\xi+T(\xi)]+[V'(\xi),\xi+T(\xi)]\\&+[V'(T(\xi)),\rho_0+\xi]+[V''(\xi,\xi),\rho_0+\xi]\\&+2[V''(T(\xi),\xi),\rho_0]+[V'''(\xi,\xi,\xi),\rho_0].\end{aligned} \tag{16}$$

The linear case ($\mathcal{R}(\xi)=0$) reproduces the well-known LR-TDDFT equations used in conventional excited state energy calculations. The oscillator modes are obtained by diagonalizing the Liouville operator

$$\mathcal{L}\xi_\alpha=\Omega_\alpha\xi_\alpha. \tag{17}$$

In the basis of Kohn–Sham orbitals Eq. (17) reproduces the so-called LR-TDDFT Casida equations

$$\begin{bmatrix}\mathbf{A}&\mathbf{B}\\\mathbf{B}^*&\mathbf{A}^*\end{bmatrix}\begin{bmatrix}X_\alpha\\Y_\alpha\end{bmatrix}=\Omega_\alpha\begin{bmatrix}\mathbf{1}&\mathbf{0}\\\mathbf{0}&-\mathbf{1}\end{bmatrix}\begin{bmatrix}X_\alpha\\Y_\alpha\end{bmatrix}, \tag{18}$$

where

$$\begin{aligned}A_{ia\sigma,jb\tau}&=\delta_{\sigma\tau}\delta_{ij}\delta_{ab}(\epsilon_{a\sigma}-\epsilon_{i\sigma})+K^{\text{TDDFT}}_{ia\sigma,jb\tau},\\B_{ia\sigma,jb\tau}&=K^{\text{TDDFT}}_{ia\sigma,bj\tau},\end{aligned} \tag{19}$$

and X_α and Y_α are the particle-hole and hole-particle components of $\xi_\alpha=[X_\alpha,Y_\alpha]^T$, respectively. In the most general case (when also hybrid functionals are allowed) the coupling matrix is given by

$$K^{\text{TDDFT}}_{ia\sigma,jb\tau}=K^{H}_{ia\sigma,jb\tau}+c_{\text{HF}}K^{X}_{ia\sigma,jb\tau}+(1-c_{\text{HF}})K^{XC}_{ia\sigma,jb\tau}, \tag{20}$$

where, in the adiabatic approximation,

$$K^{H}_{ia\sigma,jb\tau}=\int\int d\mathbf{r}d\mathbf{r}'\,\phi^*_{i\sigma}(\mathbf{r})\phi_{a\sigma}(\mathbf{r})\frac{1}{|\mathbf{r}-\mathbf{r}'|}\phi^*_{b\tau}(\mathbf{r}')\phi_{j\tau}(\mathbf{r}'), \tag{21}$$

$$K^{X}_{ia\sigma,jb\tau}=-\int\int d\mathbf{r}d\mathbf{r}'\,\phi^*_{i\sigma}(\mathbf{r})\phi_{j\tau}(\mathbf{r})\frac{1}{|\mathbf{r}-\mathbf{r}'|}\phi^*_{b\tau}(\mathbf{r}')\phi_{a\sigma}(\mathbf{r}'), \tag{22}$$

$$K^{XC}_{ia\sigma,jb\tau}=\int\int d\mathbf{r}d\mathbf{r}'\,\phi^*_{i\sigma}(\mathbf{r})\phi_{a\tau}(\mathbf{r})\frac{\delta^2E^{XC}[\rho]}{\delta\rho(\mathbf{r})\delta\rho(\mathbf{r}')}\phi^*_{b\tau}(\mathbf{r}')\phi_{j\sigma}(\mathbf{r}'), \tag{23}$$

and the parameter c_{HF} measures the amount of admixed Hartree–Fock exchange. Here, the indices i,j (a,b) run over the occupied (virtual) Kohn–Sham orbitals. The eigenstates ξ_α with the corresponding eigenvalues Ω_α come in conjugated pairs

$$\mathcal{L}\xi_\alpha=\Omega_\alpha\xi_\alpha,\quad \mathcal{L}\xi^\dagger_\alpha=-\Omega_\alpha\xi^\dagger_\alpha, \tag{24}$$

where $\alpha=1\cdots M$, and M is the dimension of the matrices $\mathbf{A}$ and $\mathbf{B}$ in Eq. (19), $M=N_{\text{occ}}\times N_{\text{virt}}$. Therefore, to each eigenstate ξ_α with frequency Ω_α there is a counterpart $\xi^\dagger_\alpha\equiv\xi_{-\alpha}$ with frequency $-\Omega_\alpha\equiv\Omega_{-\alpha}$.

III. MATRIX ELEMENTS BEYOND LINEAR RESPONSE

In this section, we describe the second-order density-density response function obtained in the framework of TDDFT and in standard many-body theory.[39] Following Refs. 36 and 38, the second-order TDDFT density response functions are given by

$$\begin{aligned}\chi^{(2)}(\omega_1,\omega_2,\mathbf{r},\mathbf{r}',\mathbf{r}'')=&\sum_{\alpha\beta\gamma}\frac{V''_{-\alpha\beta\gamma}\rho_\alpha(\mathbf{r})\rho_{-\beta}(\mathbf{r}')\rho_{-\gamma}(\mathbf{r}'')s_\alpha s_\beta s_\gamma}{(\Omega_\alpha-\omega_1-\omega_2)(\Omega_\beta-\omega_1)(\Omega_\gamma-\omega_2)}\\&-\frac{1}{2}\sum_{\alpha\beta}\frac{\rho_{-\alpha\beta}(\mathbf{r})\rho_\alpha(\mathbf{r}')\rho_{-\beta}(\mathbf{r}'')s_\alpha s_\beta}{(\Omega_\alpha-\omega_1-\omega_2)(\Omega_\beta-\omega_1)}\\&-\frac{1}{2}\sum_{\alpha\beta}\frac{\rho_{-\alpha\beta}(\mathbf{r})\rho_\alpha(\mathbf{r}')\rho_{-\beta}(\mathbf{r}'')s_\alpha s_\beta}{(\Omega_\alpha-\omega_1-\omega_2)(\Omega_\beta-\omega_2)}\\&-\frac{1}{2}\sum_{\alpha\beta}\frac{\rho_{\alpha\beta}(\mathbf{r})\rho_{-\alpha}(\mathbf{r}')\rho_{-\beta}(\mathbf{r}'')s_\alpha s_\beta}{(\Omega_\alpha-\omega_1)(\Omega_\beta-\omega_2)},\end{aligned} \tag{25}$$

where $s_\alpha=\text{sign}(\alpha)$, $\alpha,\beta,\gamma=\pm1,\pm2,\cdots$, and $V''_{\alpha\beta\gamma}$ are the second-order perturbation potentials in Eq. (6) given in terms of ξ_α,

$$\begin{aligned}V''_{\alpha\beta\gamma}=&\tfrac{1}{2}\text{Tr}[(I-2\rho_0)((\xi_\beta\xi_\gamma+\xi_\gamma\xi_\beta)V''[\xi_\alpha]\\&+(\xi_\alpha\xi_\beta+\xi_\beta\xi_\alpha)V''[\xi_\gamma]+(\xi_\alpha\xi_\gamma+\xi_\gamma\xi_\alpha)V''[\xi_\beta])],\end{aligned} \tag{26}$$

with

$$V''[\xi_\alpha](\mathbf{r})\xi_\beta=V'[\xi_\alpha](\mathbf{r})\xi_\beta+V''_{nl}[\xi_\alpha,\xi_\beta](\mathbf{r})\rho_0(\mathbf{r}), \tag{27}$$

$$V'[\xi_\alpha](\mathbf{r})=\int d\mathbf{r}'f'_{xc}[\rho_0](\mathbf{r},\mathbf{r}')\xi_\alpha(\mathbf{r}'), \tag{28}$$

$$V''_{nl}[\xi_\alpha,\xi_\beta](\mathbf{r})=\int d\mathbf{r}'\int d\mathbf{r}''g_{xc}[\rho_0](\mathbf{r},\mathbf{r}',\mathbf{r}'')\xi_\alpha(\mathbf{r}')\xi_\beta(\mathbf{r}''), \tag{29}$$

and

$$f'_{xc}[\rho_0](\mathbf{r},\mathbf{r}')=f_{xc}[\rho_0](\mathbf{r},\mathbf{r}')-\frac{1}{|\mathbf{r}-\mathbf{r}'|}. \tag{30}$$

Using the following definition of the dipole matrices:[36,40]

$$\boldsymbol{\mu}_\alpha=\text{Tr}([\rho_0,\xi_\alpha][\mu,\rho_0]), \tag{31}$$

$$\boldsymbol{\mu}_{\alpha\beta}=\text{Tr}([\rho_0,\xi_\alpha][\mu,\xi_\beta]), \tag{32}$$

the second-order polarizability within TDDFT becomes

$$\beta_r^{(ijk)}(\omega_1,\omega_2) = -\sum_{\alpha\beta\gamma=-M}^{M} \frac{V''_{-\alpha\beta\gamma}\mu_\alpha^{(i)}\mu_{-\beta}^{(j)}\mu_{-\gamma}^{(k)}s_\alpha s_\beta s_\gamma}{(\Omega_\alpha-\omega_1-\omega_2)(\Omega_\beta-\omega_1)(\Omega_\gamma-\omega_2)} + \frac{1}{2}\sum_{\alpha\beta=-M}^{M} \frac{\mu_{-\alpha\beta}^{(j)}\mu_\alpha^{(i)}\mu_{-\beta}^{(k)}s_\alpha s_\beta}{(\Omega_\alpha-\omega_1-\omega_2)(\Omega_\beta-\omega_1)} + \frac{1}{2}\sum_{\alpha\beta=-M}^{M} \frac{\mu_{-\alpha\beta}^{(j)}\mu_\alpha^{(i)}\mu_{-\beta}^{(k)}s_\alpha s_\beta}{(\Omega_\alpha-\omega_1-\omega_2)(\Omega_\beta-\omega_2)} + \frac{1}{2}\sum_{\alpha\beta=-M}^{M} \frac{\mu_{\alpha\beta}^{(i)}\mu_{-\alpha}^{(j)}\mu_{-\beta}^{(k)}s_\alpha s_\beta}{(\Omega_\alpha-\omega_1)(\Omega_\beta-\omega_2)}, \tag{33}$$

where $i,j,k \in \{x,y,z\}$, and $\boldsymbol{\mu}_{-\alpha\beta}$ is the transition dipole between states α and β for which $\boldsymbol{\mu}_\alpha = \boldsymbol{\mu}_{-\alpha}^*$ and $\boldsymbol{\mu}_{-\alpha\beta} = \boldsymbol{\mu}_{-\beta\alpha}^*$ (see also Ref. 36).

Within the many-body formulation of quantum mechanics in second quantization, the sum-over-state second-order density-density response function is obtained using a perturbative approach applied to the molecular Hamiltonian

$$H_{\mathrm{mol}} = \sum_{mn\sigma} T_{mn}\hat{c}_{m\sigma}^\dagger\hat{c}_{n\sigma} + \sum_{mnkl\sigma\tau} \langle\phi_n\phi_m|V_{ee}|\phi_k\phi_l\rangle\hat{c}_{m\sigma}^\dagger\hat{c}_{n\sigma}^\dagger\hat{c}_{k\tau}\hat{c}_{l\tau} - \mathcal{E}(t)\sum_{mn\sigma}\mu_{mn}\hat{c}_{m\sigma}^\dagger\hat{c}_{n\sigma}, \tag{34}$$

where $\hat{c}_{m\sigma}^\dagger$ ($\hat{c}_{m\sigma}$) are the creation (annihilation) operators acting on the Fock space spanned by the one-electron orbitals $\{\phi_{m\sigma}\}$, and which fulfill the Fermi anticommutation relations

$$[\hat{c}_m^\dagger,\hat{c}_n]_+ = \delta_{mn}, \quad [\hat{c}_m^\dagger,\hat{c}_n^\dagger]_+ = [\hat{c}_m,\hat{c}_n]_+ = 0, \tag{35}$$

T_{mn} is the one-body energy matrix element (kinetic plus nuclear attraction terms), $\langle\phi_n\phi_m|V_{ee}|\phi_k\phi_l\rangle$ is the Coulomb interaction, and the last term is the interaction with the external radiation field. Finally, the many-body second-order polarizability function reads

$$\beta_{sos}^{(ijk)}(\omega_1,\omega_2) = \frac{1}{2}\sum_{\alpha\beta=1}^{M}\sum_{\mathrm{perm}(\omega_1,\omega_2)}\left[\frac{\mu_\alpha^{(i)}\mu_{-\alpha\beta}^{(j)}\mu_{-\beta}^{(k)}}{(\Omega_\alpha-\omega_1-\omega_2)(\Omega_\beta-\omega_1)} + \frac{\mu_\alpha^{(i)}\mu_{-\alpha\beta}^{(j)}\mu_{-\beta}^{(k)}}{(\Omega_\alpha+\omega_2)(\Omega_\beta+\omega_1+\omega_2)} + \frac{\mu_{\alpha\beta}^{(i)}\mu_{-\alpha}^{(j)}\mu_{-\beta}^{(k)}}{(\Omega_\alpha+\omega_2)(\Omega_\beta-\omega_1)}\right], \tag{36}$$

with $\mu_\alpha^{(i)} = \langle\Psi_0|\mu^{(i)}|\Psi_\alpha^{(1)}\rangle$ and $\mu_{-\alpha\beta}^{(i)} = \langle\Psi_\alpha^{(1)}|\mu^{(i)}|\Psi_\beta^{(1)}\rangle$.

The TDDFT second-order density-density response function [Eq. (25)] can be converted into a sum-over-state representation by means of setting up of a classical system of coupled harmonic oscillators (bosons) that share the same linear and second-order response properties of TDDFT.[35,36,38] After quantizing the corresponding classical oscillator Hamiltonian, the match of the second-order response function, Eq. (33), with the many-body analog, Eq. (36), leads to the following correspondence (bosonization) of the collective fermion pairs:

$$\sum_\sigma \hat{c}_{m\sigma}^\dagger\hat{c}_{n\sigma} \to \sum_\sigma \tilde{c}_{m\sigma}^\dagger\tilde{c}_{n\sigma}, \tag{37}$$

with[41]

$$\sum_\sigma \tilde{c}_{m\sigma}^\dagger\tilde{c}_{n\sigma} = (\rho_0)_{mn} + \sum_\alpha((\xi_\alpha^\dagger)_{mn}\tilde{a}_\alpha^\dagger + (\xi_\alpha)_{mn}\tilde{a}_\alpha) + \frac{1}{2}\sum_{\alpha\beta>0}(([[\xi_\alpha^\dagger,\rho_0],\xi_\beta])_{mn}\tilde{a}_\alpha\tilde{a}_\beta + 2([[\xi_\alpha^\dagger,\rho_0],\xi_\beta])_{mn}\tilde{a}_\alpha^\dagger\tilde{a}_\beta + ([[\xi_\alpha^\dagger,\rho_0],\xi_\beta^\dagger])_{mn}\tilde{a}_\alpha^\dagger\tilde{a}_\beta^\dagger), \tag{38}$$

where the operators $\hat{c}$ and $\hat{c}^\dagger$ act on the (fermionic) Fock space spanned by the many-electron eigenfunctions of the Hamiltonian H_{mol} and the operators $\tilde{a}$ and $\tilde{a}^\dagger$ as well as $\tilde{c}$ and $\tilde{c}^\dagger$ act on the bosonic states of the quantized coupled harmonic Hamiltonian constructed to reproduce TDDFT response quantities.

This mapping leads, order by order, to the following identities:

$$\langle\Psi_0|\sum_\sigma \hat{c}_{m\sigma}^\dagger\hat{c}_{n\sigma}|\Psi_0\rangle = \langle\psi^{(0)}|\sum_\sigma \tilde{c}_{m\sigma}^\dagger\tilde{c}_{n\sigma}|\psi^{(0)}\rangle, \tag{39}$$

$$\langle\Psi_0|\sum_\sigma \hat{c}_{m\sigma}^\dagger\hat{c}_{n\sigma}|\Psi_\alpha^{(1)}\rangle = \langle\psi^{(0)}|\sum_\sigma \tilde{c}_{m\sigma}^\dagger\tilde{c}_{n\sigma}|\psi_\alpha^{(1)}\rangle, \tag{40}$$

$$\langle\Psi_0|\sum_\sigma \hat{c}_{m\sigma}^\dagger\hat{c}_{n\sigma}|\Psi_{\alpha\beta}^{(2)}\rangle = \langle\psi^{(0)}|\sum_\sigma \tilde{c}_{m\sigma}^\dagger\tilde{c}_{n\sigma}|\psi_{\alpha\beta}^{(2)}\rangle, \tag{41}$$

$$\langle\Psi_\alpha^{(1)}|\sum_\sigma \hat{c}_{m\sigma}^\dagger\hat{c}_{n\sigma}|\Psi_\beta^{(1)}\rangle = \langle\psi_\alpha^{(1)}|\sum_\sigma \tilde{c}_{m\sigma}^\dagger\tilde{c}_{n\sigma}|\psi_\beta^{(1)}\rangle, \tag{42}$$

where $|\Psi_0\rangle$, $|\Psi_\alpha^{(1)}\rangle$, and $|\Psi_{\alpha\beta}^{(2)}\rangle$ are the ground and excited state many-electron wavefunctions of the molecular Hamiltonian H_{mol} with energies E_{GS}, $E_{GS}+\Omega_\alpha$, and $E_{GS}+\Omega_\alpha+\Omega_\beta$, respectively, and $|\psi^{(0)}\rangle$, $|\psi_\alpha^{(1)}\rangle$, and $|\psi_{\alpha\beta}^{(2)}\rangle$ are the ground state, first, and second excited states of the corresponding quantum coupled oscillators. The states $|\psi^{(0)}\rangle$, $|\psi_\alpha^{(1)}\rangle$, and $|\psi_{\alpha\beta}^{(2)}\rangle$ are computed using perturbation theory to first-order in the Kohn–Sham *xc*-potential V_{xc} (see Ref. 35).

Finally, evaluation of the matrix elements in the right hand side of Eqs. (39)–(42) produces the following transition densities:

$$\langle\Psi_0|\sum_\sigma \hat{c}_{m\sigma}^\dagger\hat{c}_{n\sigma}|\Psi_0\rangle = (\rho_0)_{mn}, \tag{43}$$

$$\langle\Psi_0|\sum_\sigma \hat{c}_{m\sigma}^\dagger\hat{c}_{n\sigma}|\Psi_\alpha^{(1)}\rangle = (\xi_\alpha)_{mn}, \tag{44}$$

$$\langle\Psi_0|\sum_\sigma \hat{c}_{m\sigma}^\dagger\hat{c}_{n\sigma}|\Psi_{\alpha\beta}^{(2)}\rangle = \frac{1}{\sqrt{1+\delta_{\alpha\beta}}}\left[([[\xi_\alpha,\rho_0],\xi_\beta])_{mn} + \sum_{\gamma>0}\left(\frac{V''_{\alpha\beta-\gamma}(\xi_\gamma)_{mn}}{\Omega_\alpha+\Omega_\beta-\Omega_\gamma} - \frac{V''_{\alpha\beta\gamma}(\xi_\gamma^\dagger)_{mn}}{\Omega_\alpha+\Omega_\beta+\Omega_\gamma}\right)\right], \tag{45}$$

$$\langle \Psi_\alpha^{(1)} | \sum_\sigma \hat{c}_{m\sigma}^\dagger \hat{c}_{n\sigma} | \Psi_\beta^{(1)} \rangle = (\rho_0)_{mn}\delta_{\alpha\beta} + ([[\xi_\alpha^\dagger, \rho_0], \xi_\beta])_{mn} + \sum_{\gamma>0} \left(\frac{V''_{-\alpha\beta-\gamma}(\xi_\gamma)_{mn}}{\Omega_\beta - \Omega_\alpha - \Omega_\gamma} - \frac{V''_{\alpha-\beta-\gamma}(\xi_\gamma^\dagger)_{mn}}{\Omega_\beta - \Omega_\alpha + \Omega_\gamma} \right), \quad (46)$$

where $\xi_\alpha^\dagger = \xi_{-\alpha}$. One can prove the correctness of these correspondences by substituting Eqs. (43)–(46) into the second-order sum-over-state expression for the polarizability [Eq. (36)], which reproduces the TDDFT second-order polarizability within the TDA. Equation (46) is the starting point for the following investigation on the evaluation of matrix elements between pairs of singly excited states using LR-TDDFT.

IV. VALIDITY OF SECOND-ORDER RESPONSE QUANTITIES COMPUTED FROM LR-TDDFT AUXILIARY MANY-ELECTRON WAVEFUNCTIONS

The main objective of this paper is the validation of the method introduced in Refs. 31 and 34 for the computation of matrix elements of one-body operators using auxiliary singly excited Slater determinants of Kohn–Sham orbitals. We start considering the calculation of the matrix element of a one-body operator, $\mathcal{O}$, taken between the ground state and an excited singlet state with excitation energy Ω_α. Note that the NACVs are obtained identifying $\mathcal{O}$ with the vector operator $\nabla_{\boldsymbol{R}} H_{\mathrm{KS}}$, where $\boldsymbol{R}$ is the collective vector of the nuclear positions. Using the method described in Ref. 31 and $c_{ia}^\alpha = \sqrt{\epsilon_a - \epsilon_i}/\Omega_\alpha e_{ia}^\alpha$, the matrix element is evaluated as

$$\sigma_{0\alpha} = \sum_{ia} c_{ia}^\alpha \langle \Psi_0 | \mathcal{O} | \Psi_{i\to a}^\alpha \rangle = \sum_{ia} c_{ia}^\alpha \langle \phi_i | \mathcal{O} | \psi_a \rangle = \sum_{ia} \sqrt{\frac{\epsilon_a - \epsilon_i}{\Omega_\alpha}} e_{ia}^\alpha \langle \phi_i | \mathcal{O} | \psi_a \rangle, \quad (47)$$

where Ψ_0 and $\Psi_{i\to a}^\alpha$ are the LR-TDDFT auxiliary many-electron wavefunctions, and $\{\phi_{i\sigma}(r)\}_{i=1}^N$ and $\{\psi_{a\sigma}(r)\}_{a=1}^\infty$ are the occupied and virtual (unoccupied) KS orbitals, respectively, with corresponding occupations $f_{i\sigma}=1$ and $f_{a\sigma}=0$. In the particle-hole $(p-h)$, hole-particle $(h-p)$ formulation of the LR-TDDFT equations[1,42] we have

$$e_{ia}^\alpha = \sqrt{\Omega_\alpha}[(A-B)^{-1/2}(X_\alpha + Y_\alpha)]_{ia}, \quad (48)$$

or equivalently

$$e_{ia}^\alpha = \frac{1}{\sqrt{\Omega_\alpha}}[(A-B)^{1/2}(X_\alpha - Y_\alpha)]_{ia}, \quad (49)$$

and therefore

$$\sigma_{0\alpha} = \sum_{ia} (X_\alpha + Y_\alpha)_{ia} \langle \phi_i | \mathcal{O} | \psi_a \rangle = \sum_{ia} (X_\alpha + Y_\alpha)_{ia} \mathcal{O}_{ai}^T, \quad (50)$$

since the matrix $(\boldsymbol{A}-\boldsymbol{B})^{-1/2}$ is diagonal with elements $[(A-B)^{-1/2}]_{ia,jb} = \delta_{i,j}\delta_{a,b}\sqrt{1/\epsilon_a - \epsilon_i}$ $(\mathcal{O}_{ia} = \langle \phi_i | \mathcal{O} | \psi_a \rangle)$. On the other hand, using the coupled electronic oscillator approach summarized above, the same matrix element can be written as

$$\sigma_{0\alpha} = Tr(\mathcal{O}\xi_\alpha) = \sum_{pq} \mathcal{O}_{pq}\xi_{qp}^\alpha = \sum_{ia} (\mathcal{O}_{ai}^T X_{ia}^\alpha + \mathcal{O}_{ia} Y_{ai}^{\alpha T}), \quad (51)$$

where $p,q = 1,\ldots,M$ and $M = N_{\mathrm{occ}} + N_{\mathrm{virt}}$ (see also Ref. 29).

Having proven the equivalence of the two approaches for the case of a matrix element involving the ground state and one excited state $\langle \Psi_0 | \mathcal{O} | \Psi_{i\to a}^\alpha \rangle$, we move to the more interesting case of a matrix element of the kind $\langle \Psi_{i\to a}^\alpha | \mathcal{O} | \Psi_{j\to b}^\beta \rangle$, which is beyond reach of linear response theory.

Applying the LR-TDDFT auxiliary many-electron wavefunction approach to the matrix element $\sigma_{\alpha,\beta} = \langle \Psi^\alpha | \mathcal{O} | \Psi^\beta \rangle$ gives

$$\sigma_{\alpha,\beta} = \sum_{ia}\sum_{jb} c_{ia}^{\alpha\dagger} c_{jb}^\beta \langle \Psi_{i\to a}^\alpha | \mathcal{O} | \Psi_{j\to b}^\beta \rangle. \quad (52)$$

In the case $\mathcal{O}$ is a one-body operator of the form $\mathcal{O} = \Sigma_{pq} \mathcal{O}_{pq} \hat{c}_p^\dagger \hat{c}_q$, the only nonzero matrix elements are of the type $\langle \Psi_{i\to a}^\alpha | \mathcal{O} | \Psi_{i\to b}^\beta \rangle$ and $\langle \Psi_{i\to a}^\alpha | \mathcal{O} | \Psi_{j\to a}^\beta \rangle$ and therefore

$$\sigma_{\alpha,\beta} = \sum_{iab} c_{ia}^{\alpha\dagger} c_{ib}^\beta \langle \psi_a | \mathcal{O} | \psi_b \rangle - \sum_{aij} c_{ia}^{\alpha\dagger} c_{ja}^\beta \langle \phi_i | \mathcal{O} | \phi_j \rangle. \quad (53)$$

Using $c_{ia}^\alpha = \sqrt{\epsilon_a - \epsilon_i/\Omega_\alpha} e_{ia}^\alpha$ and Eq. (48) we finally get

$$\sigma_{\alpha,\beta} = \sum_{iab} \sqrt{\frac{\epsilon_a - \epsilon_i}{\Omega_\alpha}} \sqrt{\frac{\epsilon_b - \epsilon_i}{\Omega_\beta}} e_{ia}^{\alpha\dagger} e_{ib}^\beta \mathcal{O}_{ab} - \sum_{aij} \sqrt{\frac{\epsilon_a - \epsilon_i}{\Omega_\alpha}} \sqrt{\frac{\epsilon_a - \epsilon_j}{\Omega_\beta}} e_{ia}^{\alpha\dagger} e_{ja}^\beta \mathcal{O}_{ij}, \quad (54)$$

and therefore [since the matrix $(\boldsymbol{A}-\boldsymbol{B})^{-1/2}$ is diagonal],

$$\sigma_{\alpha,\beta} = \sum_{iab} (X_{ia}^\alpha + Y_{ia}^\alpha)^\dagger (X_{ib}^\beta + Y_{ib}^\beta) \mathcal{O}_{ab} - \sum_{aij} (X_{ia}^\alpha + Y_{ia}^\alpha)^\dagger (X_{ja}^\beta + Y_{ja}^\beta) \mathcal{O}_{ij}. \quad (55)$$

For a Hermitian and real (symmetric) operator $\mathcal{O}$ we get

$$\sigma_{\alpha,\beta} = \sum_{iab} (X_{ai}^{\alpha\dagger} X_{ib}^\beta + X_{ai}^{\alpha\dagger} Y_{ib}^\beta + Y_{ai}^{\alpha\dagger} X_{ib}^\beta + Y_{ai}^{\alpha\dagger} Y_{ib}^\beta) \mathcal{O}_{ab} - \sum_{aij} (X_{ai}^{\alpha\dagger} X_{ja}^\beta + X_{ai}^{\alpha\dagger} Y_{ja}^\beta + Y_{ai}^{\alpha\dagger} X_{ja}^\beta + Y_{ai}^{\alpha\dagger} Y_{ja}^\beta) \mathcal{O}_{ij} \quad (56)$$

$$= \sum_{ab} (X^{\alpha\dagger} X^\beta + X^{\alpha\dagger} Y^\beta + Y^{\alpha\dagger} X^\beta + Y^{\alpha\dagger} Y^\beta)_{ab} \mathcal{O}_{ba} - \sum_{ij} (X^\beta X^{\alpha\dagger} + Y^\beta X^{\alpha\dagger} + X^\beta Y^{\alpha\dagger} + Y^\beta Y^{\alpha\dagger})_{ji} \mathcal{O}_{ij}. \quad (57)$$

In matrix notation, we finally get (after cyclic permutation of the trace)

$$\sigma_{\alpha,\beta} = [\mathrm{Tr}_v(\boldsymbol{X}_\beta \mathcal{O}_v \boldsymbol{X}_\alpha^\dagger) + \mathrm{Tr}_v(\boldsymbol{Y}_\beta \mathcal{O}_v \boldsymbol{X}_\alpha^\dagger) + \mathrm{Tr}_v(\boldsymbol{X}_\beta \mathcal{O}_v \boldsymbol{Y}_\alpha^\dagger) + \mathrm{Tr}_v(\boldsymbol{Y}_\beta \mathcal{O}_v \boldsymbol{Y}_\alpha^\dagger)] - [\mathrm{Tr}_o(\boldsymbol{X}_\alpha^\dagger \mathcal{O}_o \boldsymbol{X}_\beta) + \mathrm{Tr}_o(\boldsymbol{X}_\alpha^\dagger \mathcal{O}_o \boldsymbol{Y}_\beta) + \mathrm{Tr}_o(\boldsymbol{Y}_\alpha^\dagger \mathcal{O}_o \boldsymbol{X}_\beta) + \mathrm{Tr}_o(\boldsymbol{Y}_\alpha^\dagger \mathcal{O}_o \boldsymbol{Y}_\beta)], \quad (58)$$

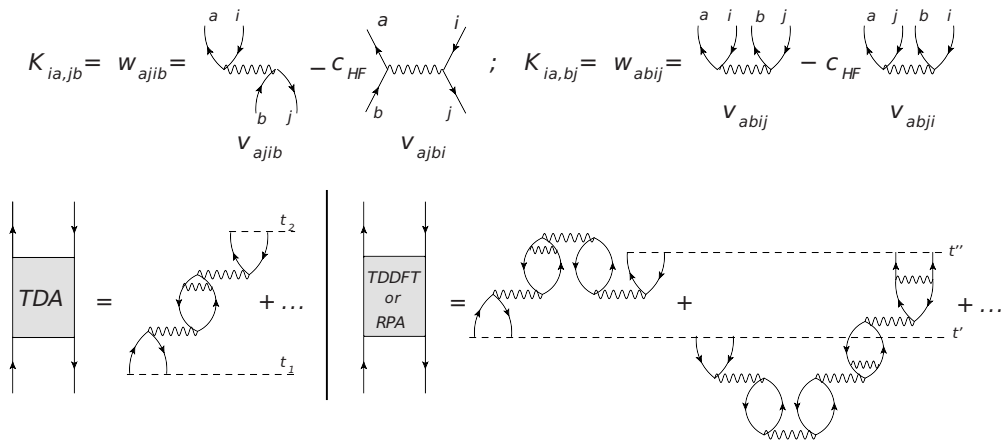

FIG. 1. Upper panel: diagrammatic representation of the matrix elements $K_{ia,jb}$ and $K_{ia,bj}$ constituting matrices $\boldsymbol{A}$ and $\boldsymbol{B}$, respectively. The matrix elements are also given in the "physics" notation (w_{ajib} and w_{abij}), which allows a more direct translation into Feynman graphs (see for instance Refs. 45 and 64). Lower panel: polarization propagator in the TDA (left) and in the full TDDFT linear response case (right). The contribution of the additional K^{XC} term in Eq. (23) is not shown (see Ref. 65). The contribution of double excitations to the full response is illustrated in the second diagram for the TDDFT polarization propagator (also valid in RPA).

where Tr_o and Tr_v represent the trace over the occupied and virtual orbitals, respectively.

We now consider the calculation of the matrix element $\sigma_{\alpha,\beta}$ within the density-matrix response approach. Using Eq. (46) together with the relation $[[\rho_0,\xi_\alpha],\xi_\beta]=(1-2\rho_0)\times(\xi_\alpha\xi_\beta+\xi_\beta\xi_\alpha)$ we first get (excluding exchange-correlation coupling terms depending on $V''_{\alpha\beta\gamma}$, which is zero in the TDA)

$$\sigma_{\alpha,\beta}=\mathrm{Tr}([[\rho_0,\xi_{-\alpha}],\xi_\beta]\mathcal{O}) = \mathrm{Tr}(\mathcal{O}(1-2\rho_0)(\xi_{-\alpha}\xi_\beta+\xi_\beta\xi_{-\alpha})). \tag{59}$$

Applying the following matrix representation in the basis of the occupied and virtual Kohn–Sham orbitals:

$$\xi_\alpha=\begin{bmatrix}\mathbf{0} & \mathbf{X}_\alpha\\ \mathbf{Y}_\alpha^\dagger & \mathbf{0}\end{bmatrix},\quad \xi_{-\alpha}=\xi_\alpha^\dagger=\begin{bmatrix}\mathbf{0} & \mathbf{Y}_\alpha\\ \mathbf{X}_\alpha^\dagger & \mathbf{0}\end{bmatrix}, \tag{60}$$

$$\xi_{-\alpha}\xi_\beta=\begin{bmatrix}\mathbf{Y}_\alpha\mathbf{Y}_\beta^\dagger & \mathbf{0}\\ \mathbf{0} & \mathbf{X}_\alpha^\dagger\mathbf{X}_\beta\end{bmatrix},\quad \xi_\beta\xi_{-\alpha}=\begin{bmatrix}\mathbf{X}_\beta\mathbf{X}_\alpha^\dagger & \mathbf{0}\\ \mathbf{0} & \mathbf{Y}_\beta^\dagger\mathbf{Y}_\alpha\end{bmatrix}, \tag{61}$$

$$\mathcal{O}=\begin{bmatrix}\mathcal{O}_o & \mathcal{O}_{ov}\\ \mathcal{O}_{vo} & \mathcal{O}_v\end{bmatrix},\quad (1-2\rho_0)=\begin{bmatrix}-\mathbf{1} & \mathbf{0}\\ \mathbf{0} & \mathbf{1}\end{bmatrix}, \tag{62}$$

we obtain

$$\sigma_{\alpha,\beta}=-\mathrm{Tr}_o(\mathcal{O}_o\boldsymbol{Y}_\alpha\boldsymbol{Y}_\beta^\dagger)+\mathrm{Tr}_v(\mathcal{O}_v\boldsymbol{X}_\alpha^\dagger\boldsymbol{X}_\beta)-\mathrm{Tr}_o(\mathcal{O}_o\boldsymbol{X}_\beta\boldsymbol{X}_\alpha^\dagger) +\mathrm{Tr}_v(\mathcal{O}_v\boldsymbol{Y}_\beta^\dagger\boldsymbol{Y}_\alpha), \tag{63}$$

and, applying the cyclic permutation rule for the trace, we get

$$\sigma_{\alpha,\beta}=-\mathrm{Tr}_o(\boldsymbol{Y}_\beta^\dagger\mathcal{O}_o\boldsymbol{Y}_\alpha)+\mathrm{Tr}_v(\boldsymbol{X}_\beta\mathcal{O}_v\boldsymbol{X}_\alpha^\dagger)-\mathrm{Tr}_o(\boldsymbol{X}_\alpha^\dagger\mathcal{O}_o\boldsymbol{X}_\beta) +\mathrm{Tr}_v(\boldsymbol{Y}_\alpha\mathcal{O}_v\boldsymbol{Y}_\beta^\dagger). \tag{64}$$

Comparing Eq. (58) with Eq. (64), we observe that the two approaches agree in the particle-hole and hole-particle sectors, while the approach based on the auxiliary wavefunctions produces additional mixed terms of the form $\boldsymbol{X}_\alpha\mathcal{O}\boldsymbol{Y}_\beta$.

It is worth mentioning that the EMS model used by Tretiak, Chernyak, and Mukamel to construct first, second, and higher order response quantities, as well as variational approaches based on a Slater determinant of Kohn–Sham orbitals,[43] do not exploit the full response space as many-body random phase approximation (RPA) and LR-TDDFT do. In particular, both methods do not take into account the possibility of adding (static) correlations to the ground state. As in many-body RPA, which differs from LR-TDDFT in the way the kernel is defined

$$K^{\mathrm{RPA}}_{ia\sigma,jb\tau}=K^H_{ia\sigma,jb\tau}+K^X_{ia\sigma,jb\tau}, \tag{65}$$

the physical meaning of the elements of matrix **B** is to add correlation in the ground state. In the diagrammatic picture, the exchange of indices in the coupling elements $K_{ia,bj}$ of matrix **B** with respect to the corresponding terms $K_{ia,jb}$ in matrix **A**, corresponds to the spontaneous generation of $2p-2h$ excitations in the ground state.[44–46] This is evident when we associate the different terms (direct term and exchange, if present) of the matrix elements $K_{ia,jb}$, in $\boldsymbol{A}$, and $K_{ia,bj}$, in $\boldsymbol{B}$ to the corresponding diagrams as shown in the upper panel of Fig. 1. Once more, only the full TDDFT linear response case (as in RPA) contains, in addition to the direct and exchange terms of matrix $\boldsymbol{A}$, the graphs responsible for virtual $2p-2h$ excitations. In the lower panel of Fig. 1 we illustrate the effect of these additional terms on the polarization propagator that describes the time evolution of a *ph* pair from time t_1 (when it is created) to time t_2 (when it is annihilated). The second graph on the right shows the case in which a singly excited *ph* state is created from a $2p-2h$ virtual excitation by the annihilation of a *ph* at time t', which also contributes to the polarization propagator. The additional terms of the form $\boldsymbol{X}_\alpha\mathcal{O}\boldsymbol{Y}_\beta$ in Eq. (58) originate therefore from the possibility in RPA and full linear response TDDFT to generate singly excited states through the de-excitation of the "correlated" ground state.

In the EMS approach, the term $\boldsymbol{X}_\alpha\mathcal{O}\boldsymbol{Y}_\beta$ would correspond to $\mathrm{Tr}([[\rho_0,\xi_\alpha],\xi_\beta]\mathcal{O})$ but it is not present in Eq. (59) because it is not allowed by construction (choice of the

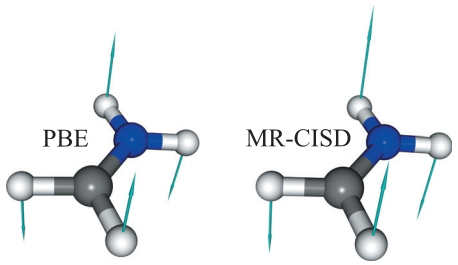

FIG. 2. NACVs of protonated formaldimine computed for the states S_1/S_2 at a common ground state optimized geometry (see computational details). Left: LR-TDDFT/TDA/PBE vectors. Right: reference MR-CISD vectors (carbon atom in gray, nitrogen atom in blue, and hydrogen atoms in white).

ground state). We therefore believe that the additional terms in Eq. (58) are physical and should also be taken into account in the calculation of second-order response quantities. What is missing in our approach, while it is present in EMS, is the correct description of the perturbation terms proportional to the anharmonic couplings $V''_{\alpha\beta\gamma}$ [Eq. (46)].

In conclusion, we observe that within the TDA (for which $\boldsymbol{Y}=0$) Eqs. (64) and (58) reduces to

$$\sigma_{\alpha,\beta} = \mathrm{Tr}_v(\boldsymbol{X}_\beta \mathcal{O}_v \boldsymbol{X}_\alpha^\dagger) - \mathrm{Tr}_o(\boldsymbol{X}_\alpha^\dagger \mathcal{O}_o \boldsymbol{X}_\beta) \tag{66}$$

and therefore both approaches (EMS and the one introduced in this work) give exactly the same matrix elements between singly excited states.

V. APPLICATION

In this section, we present a comparison between NACVs computed using LR-TDDFT/TDA within the auxiliary many-electron wavefunction approach[31,34] and high-level *ab initio* wavefunction calculations, multireference configuration interaction singles doubles (MR-CISD),[47,48] between two excited states of the simple molecule protonated formaldimine. MR-CISD is used here as a reference, taking into account both static and dynamic correlation of the electrons. The LR-TDDFT NACVs, $\mathbf{d}_{IJ}$, between two electronic states I and J are computed using Eq. (58) in the full linear response case and Eq. (66) in the TDA, where $\mathcal{O}$ is replaced by the vector operator $\nabla_{\boldsymbol{R}} H_{\mathrm{KS}}$ and $\boldsymbol{R}$ is the collective vector of the nuclear positions.

As a model system, we consider the coupling vector between the first ($S_1: \sigma \rightarrow \pi^*$) and the second excited state ($S_2: \pi \rightarrow \pi^*$) in protonated formaldimine.

For the symmetric geometry (C_{2v}) shown in Fig. 2, the difference in energy between these two states predicted by LR-TDDFT/TDA/PBE and MR-CISD is $\Delta E_{21}=2.50$ eV and $\Delta E_{21}=0.85$ eV, respectively. Despite the large difference in energy, the character of the orbitals involved in the transitions, which is crucial for the calculation of the NACVs, is similar in both approaches. Visual inspection of NACVs obtained using LR-TDDFT/TDA and MR-CISD (Fig. 2) reveals good agreement between the two methods, further confirmed by the values of the root mean square deviation rms $=0.005$ bohr^{-1} and of the average correlation $C=0.947$ obtained according to Eqs. (67) and (68), respectively (see computational details). Both NACVs describe a twist around the CN bond driven by the four hydrogen atoms. The largest deviation of the correlation is observed for the nitrogen atom ($C_N=0.717$), whereas a perfect correlation between LR-TDDFT and MR-CISD can be observed for the hydrogen atoms ($C_H>0.999$ in all four cases). In Table I we compare the quality of the NACVs computed with LR-TDDFT/TDA using different *xc*-functionals: LDA, PBE, BLYP, BP, and the hybrids B3LYP and PBE0. As in the case of PBE, the agreement with the reference MR-CISD calculation is very good for all GGA functionals, with the hybrid functionals (B3LYP and PBE0) performing slightly better. Surprisingly, among all tested functionals LDA shows the best correlation with the reference NACVs, even though this is only the case for the symmetric structure shown in Fig. 2.

In order to investigate the effect of the symmetry on the NACVs, we have performed an additional series of calculations on a geometry with a pyramidalization angle of 12° at the nitrogen atom. Pyramidalization at the CN double bond introduces some multireference character in the description of the states and therefore is limiting the accuracy of the LR-TDDFT calculations. For this reason, we could not extend our investigation to larger values of the pyramidalization angle. The computed LR-TDDFT/TDA and MR-CISD NACVs are shown in Fig. 3, while Table II reports the corresponding root mean square (rms) deviations and correlation values. Also in this case, the agreement between the NACVs computed within LR-TDDFT/TDA and MR-CISD is good, especially when hybrid functionals are used. In particular, the antiphase displacement of the carbon and nitrogen atoms is captured, although there is still some discrepancy in the vector lengths. We also observe that, compared to the

TABLE I. NACVs between states S_1 and S_2 computed for the ground state geometry of protonated formaldimine (see Fig. 3) computed using LR-TDDFT/TDA with different *xc*-functionals. MR-CISD is used as reference. The rms of the collective ($3N=18$) dimensional NACVs is computed according to Eq. (67), where $N=6$ is the number of atoms. $\mathbf{C}$ is the global correlation between the LR-TDDFT/TDA and the reference collective NACVs, $\mathbf{C}_H$ the collective correlation for the hydrogen atoms, $\mathbf{C}_N$ the correlation at nitrogen atom, and $\mathbf{C}_C$ the correlation at the carbon atom.

xc-functional	rms (bohr^{-1})	$\mathbf{C}$	$\mathbf{C}_\mathrm{H}$	$\mathbf{C}_\mathrm{N}$	$\mathbf{C}_\mathrm{C}$
LDA	0.0002	0.975	>0.999	0.882	0.970
PBE	0.0046	0.947	>0.999	0.717	0.966
BLYP	0.0005	0.900	>0.999	0.646	0.728
BP	0.0047	0.937	>0.999	0.694	0.929
B3LYP	0.0002	0.951	>0.999	0.782	0.927
PBE0	0.0041	0.940	>0.999	0.970	0.672

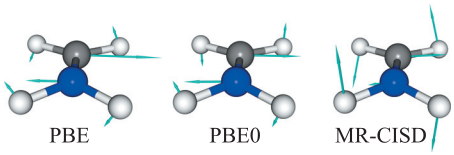

FIG. 3. NACVs of protonated formaldimine computed for the states S_1/S_2 at a geometry with a pyramidalization angle of 12° at nitrogen atom (see computational details). From the left: LR-TDDFT/TDA/PBE, LR-TDDFT/TDA/PBE0, and MR-CISD vectors (carbon atom in gray, nitrogen atom in blue, and hydrogen atoms in white).

TDA calculations, the use of the full TDDFT linear response slightly improves the agreement with the reference.

It is important to mention that, while the equations for the calculation of the NACVs in LR-TDDFT/TDA are formally exact, there are a series of approximations that are generally assumed in most conventional DFT and LR-TDDFT calculations. In particular, we used approximated DFT *xc*-functionals for the computation of all ground state properties, and we applied the so-called adiabatic approximation in the evaluation of the LR-TDDFT kernel. This last approximation implies that both matrices $\boldsymbol{A}$ and $\boldsymbol{B}$ in the set of LR-TDDFT equations [Eq. (18)] are considered frequency independent. One can expect a further improvement of the LR-TDDFT NACVs quality using for example *xc*-functionals that reproduce the correct long-range (asymptotic) behavior (see for instance Ref. 49). The use of these approximations of the *xc*-potential and LR-TDDFT kernel has however the important advantage of making the calculation of excited state energies, forces and NACVs computationally very efficient and is therefore suited for the calculation of nuclear trajectories in a nonadiabatic molecular dynamics scheme such as trajectory surface hopping (TSH).[13,27,32]

A. Computational details

The ground state geometry (Fig. 2) of protonated formaldimine was obtained using DFT/M06 calculations with an aug-cc-pVDZ (Ref. 50) basis set using the package GAUSSIAN09.[51] The distorted geometry in Fig. 2 was obtained by imposing a pyramidalization angle of 12° measured between the planes defined by the fragments H_2C and NH_2.

To compare the results obtained using different *xc*-functionals, the rms between vectors $\boldsymbol{v}$ and $\boldsymbol{v}'$ computed with two different approaches is evaluated according to

$$\mathrm{rms} = \frac{1}{3N}\sqrt{\sum_k \sum_\alpha (v_{k,\alpha} - v'_{k,\alpha})^2}, \tag{67}$$

where N is the number of atoms and α represents a Cartesian coordinate $(\alpha = x,y,z)$ of a given atom labeled by the index k. The correlation function

$$\mathrm{C}_k = \frac{\boldsymbol{v}'_k \cdot \boldsymbol{v}_k}{|\boldsymbol{v}'_k| \cdot |\boldsymbol{v}_k|} \tag{68}$$

is used to quantify the deviation between two vectors, $\boldsymbol{v}_k$ and $\boldsymbol{v}'_k$, associated with a given atomic species k computed at different levels of theory.

LR-TDDFT NACVs calculations were performed with the plane wave code CPMD (Ref. 52) within the Tamm–Dancoff approximation. The Perdew–Burke–Ernzerhof[53] (PBE), Becke[54]/Lee–Yang–Parr[55] (BLYP), Local density approximation (LDA), Becke/Perdew[56] (BP), Becke three parameter[57]/Lee–Yang–Parr (B3LYP), and PBE0 (Ref. 58) *xc*-functionals were used for both cases. Plane waves with a cutoff of 70 Ry were employed to expand the valence electrons in a box of $11 \times 11 \times 11$ Å^3. Core electrons were replaced by norm-conserving pseudopotentials of the Martins–Troullier type.[59] A convergence criteria of 10^{-7} a.u. was used for the optimization of Kohn–Sham orbitals.

MR-CISD NACVs were performed with the COLUMBUS Quantum Chemistry package.[47,48,60] Protonated formaldimine was computed starting from a CASSCF(4,3) calculation using the aug-cc-pVDZ basis set. The active space consists of the last σ and π orbitals in addition to a π^* orbital. The first three electronic states were taken into account in a state-averaged (SA) procedure with an equal weight between the states. Based on the SA-3-CASSCF(4,3) reference wavefunction, we performed an MR-CISD nonadiabatic coupling vector calculation as implemented in the COLUMBUS package. The computed NACVs include both CI and SCF contributions.

VI. CONCLUSIONS

In this paper we studied the correspondence between the NACVs computed within LR-TDDFT using the coupled electronic oscillator approach of Refs. 35 and 36 and the auxiliary many-electron wavefunctions method outlined in

TABLE II. NACVs between states S_1 and S_2 computed for a distorted geometry of protonated formaldimine using LR-TDDFT/TDA with different *xc*-functional (see Fig. 3). MR-CISD is used as reference unless specified otherwise. The rms deviation of the collective ($3N=18$) dimensional NACVs is computed according to Eq. (67), where $N=6$ is the number of atoms. **C** is the global correlation between the LR-TDDFT/TDA and the reference collective NACVs, $\mathbf{C}_\mathrm{H}$ is the collective correlation for the hydrogen atoms, $\mathbf{C}_\mathrm{N}$ is the correlation at the nitrogen atom, and $\mathbf{C}_\mathrm{C}$ is the correlation at the carbon atom.

xc-functional	rms (bohr^{-1})	**C**	$\mathbf{C}_\mathrm{H}$	$\mathbf{C}_\mathrm{N}$	$\mathbf{C}_\mathrm{C}$
LDA	0.0052	0.835	0.768	0.961	0.981
PBE	0.0037	0.911	0.881	0.962	0.983
BLYP	0.0026	0.946	0.932	0.965	0.986
BP	0.0032	0.926	0.903	0.962	0.984
B3LYP	0.0020	0.948	0.931	0.974	0.987
PBE0	0.0021	0.943	0.925	0.971	0.986
TDA/PBE versus full LR-TDDFT/PBE	0.0024	0.949	0.924	0.997	0.998

Refs. 31 and 34. We showed that this correspondence becomes exact in the case of matrix elements evaluated between ground state and singly excited states, as well as between any pair of excited states when the TDA is used. In the full linear response case, our approach produces additional terms related to the correlation of the ground state, which are not present in the EMS scheme. These terms contribute to the matrix elements for singly excited states, through the de-excitation of $2p-2h$ states generated by elements of the $\boldsymbol{B}$ matrix [Eq. (19)]. On the other end, pure second-order terms proportional to the anharmonic couplings $V''_{\alpha\beta\gamma}$ of Eq. (46) are neglected in our formalism.

Despite the *in principle* exact nature of LR-TDDFT, a number of approximations are required in order to perform calculations on realistic molecules and condensed phase systems. These include approximations of the exchange-correlation functional and of the LR-TDDFT kernel, which is usually taken as frequency independent (adiabatic approximation).

In order to study the effects of these approximations on the quality of the NACVs computed between pairs of molecular excited states, we presented results obtained for protonated formaldimine using LR-TDDFT with different *xc*-functionals and compared the outcome with MR-CISD calculations. In addition, we also studied the effect of using the full linear response calculations instead of invoking the TDA. In this case, the NACVs are computed according to Eq. (58), which includes terms of the form $\boldsymbol{X}_\alpha \mathcal{O} \boldsymbol{Y}_\beta$ that arise from $2p-2h$ excitations of the ground state and that are not taken into account in the EMS approach.

Our results show that LR-TDDFT/TDA can reproduce with a very good degree of accuracy the direction of NACVs associated with the different nuclei for both the fully symmetric (C_{2v}) and the slightly distorted geometry shown in Figs. 2 and 3. The performance of the different functionals (LDA, GGAs, and hybrids) is in general equally good, with a small improvement when exact exchange is included. The use of the full TDDFT linear response scheme does not alter the results significantly and produces NACVs that well correlate with the TDA results, meaning that TDA is a good approximation also in the calculation of the NACVs.

We believe that the calculation of NACVs between excited states using LR-TDDFT combined with a scheme for nonadiabatic molecular dynamics,[13,61–63] like for instance TSH, will give an important boost to the study of the photophysics and photochemistry of large molecular systems.

[1] M. E. Casida, in *Recent Advances in Density Functional Methods*, edited by D. P. Chong (World Scientific, Singapore, 1995), p. 155.
[2] M. Petersilka, U. J. Gossmann, and E. K. U. Gross, Phys. Rev. Lett. **76**, 1212 (1996).
[3] E. K. U. Gross and W. Kohn, Phys. Rev. Lett. **55**, 2850 (1985).
[4] H. Appel, E. K. U. Gross, and K. Burke, Phys. Rev. Lett. **90**, 043005 (2003).
[5] S. Hirata and M. Head-Gordon, Chem. Phys. Lett. **314**, 291 (1999).
[6] J. Hutter, J. Chem. Phys. **118**, 3928 (2003).
[7] U. F. Röhrig, I. Frank, J. Hutter, A. Laio, J. VandeVondele, and U. Rothlisberger, ChemPhysChem **4**, 1177 (2003).
[8] L. Bernasconi, M. Sprik, and J. Hutter, J. Chem. Phys. **119**, 12417 (2003).
[9] G. Onida, L. Reining, and A. Rubio, Rev. Mod. Phys. **74**, 601 (2002).
[10] I. Tavernelli, Phys. Rev. B **73**, 094204 (2006).
[11] I. Tavernelli, M. Gaigeot, R. Vuilleumier, C. Stia, M. A. H. Penhoat, and M. F. Politis, ChemPhysChem **9**, 2099 (2008).
[12] I. Tavernelli, U. F. Röhrig, and U. Rothlisberger, Mol. Phys. **103**, 963 (2005).
[13] E. Tapavicza, I. Tavernelli, U. Rothlisberger, C. Filippi, and M. E. Casida, J. Chem. Phys. **129**, 124108 (2008).
[14] M. Cascella, M. A. Cuendet, I. Tavernelli, and U. Rothlisberger, J. Phys. Chem. B **111**, 10248 (2007).
[15] A. Dreuw, J. Weisman, and M. Head-Gordon, J. Chem. Phys. **119**, 2943 (2003).
[16] S. Grimme and M. Parac, Comput. Phys. Commun. **3**, 292 (2003).
[17] M. Wanko, M. Garavelli, F. Bernardi, T. A. Niehaus, T. Fraunheim, and M. Elstner, J. Chem. Phys. **120**, 1674 (2004).
[18] S. J. A. van Gisbergen, P. R. T. Schipper, O. V. Gritsenko, E. J. Baerends, J. G. Snijders, B. Champagne, and B. Kirtman, Phys. Rev. Lett. **83**, 694 (1999).
[19] O. V. Gritsenko, S. J. A. van Gisbergen, A. Görling, and E. J. Baerends, J. Chem. Phys. **113**, 8478 (2000).
[20] M. E. Casida, F. Gutierrez, J. Guan, F.-X. Gadea, D. R. Salahub, and J.-P. Daudey, J. Chem. Phys. **113**, 7062 (2000).
[21] B. G. Levine, C. Ko, J. Quenneville, and T. J. Martinez, Mol. Phys. **104**, 1039 (2006).
[22] F. Furche and R. Ahlrichs, J. Chem. Phys. **117**, 7433 (2002).
[23] J. C. Tully, in *Modern Methods for Multidimensional Dynamics Computations in Chemistry*, edited by D. L. Thompson (World Scientific, Singapore, 1998).
[24] J. C. Tully, J. Chem. Phys. **93**, 1061 (1990).
[25] M. Ben-Nun, J. Quenneville, and T. J. Martinez, J. Phys. Chem. A **104**, 5161 (2000).
[26] N. L. Doltsinis and D. Marx, Phys. Rev. Lett. **88**, 166402 (2002).
[27] E. Tapavicza, I. Tavernelli, and U. Rothlisberger, Phys. Rev. Lett. **98**, 023001 (2007).
[28] M. Barbatti, A. J. A. Aquino, and H. Lischka, Mol. Phys. **104**, 1053 (2006).
[29] V. Chernyak and S. Mukamel, J. Chem. Phys. **112**, 3572 (2000).
[30] R. Baer, Chem. Phys. Lett. **364**, 75 (2002).
[31] I. Tavernelli, E. Tapavicza, and U. Rothlisberger, J. Chem. Phys. **130**, 124107 (2009).
[32] I. Tavernelli, E. Tapavicza, and U. Rothlisberger, J. Mol. Struct.: THEOCHEM **914**, 22 (2009).
[33] C. P. Hu, H. Hirai, and O. Sugino, J. Chem. Phys. **127**, 064103 (2007).
[34] I. Tavernelli, B. F. E. Curchod, and U. Rothlisberger, J. Chem. Phys. **131**, 196101 (2009).
[35] S. Tretiak, V. Chernyak, and S. Mukamel, Int. J. Quantum Chem. **70**, 711 (1998).
[36] S. Tretiak and V. Chernyak, J. Chem. Phys. **119**, 8809 (2003).
[37] V. Chernyak and S. Mukamel, J. Chem. Phys. **111**, 4383 (1999).
[38] O. Berman and S. Mukamel, Phys. Rev. A **67**, 042503 (2003).
[39] B. J. Orr and J. F. Ward, Mol. Phys. **20**, 513 (1971).
[40] S. Tretiak and S. Mukamel, Chem. Rev. (Washington, D.C.) **102**, 3171 (2002).
[41] S. Mukamel and O. Berman, J. Chem. Phys. **119**, 12194 (2003).
[42] F. Furche, J. Chem. Phys. **114**, 5982 (2001).
[43] T. Ziegler, M. Seth, M. Krykunov, J. Autschbach, and F. Wang, J. Chem. Phys. **130**, 154102 (2009).
[44] D. J. Thouless, Nucl. Phys. **22**, 78 (1961).
[45] A. L. Fetter and J. D. Walecka, *Quantum Theory of Many-Particle Systems* (McGraw-Hill, New York, 1971).
[46] P. Ring and P. Schuck, *The Nuclear Many-Body Problem* (Springer-Verlag, Berlin, 2004).
[47] H. Lischka, M. Dallos, P. G. Szalay, D. R. Yarkony, and R. Shepard, J. Chem. Phys. **120**, 7322 (2004).
[48] M. Dallos, H. Lischka, R. Shepard, D. R. Yarkony, and P. G. Szalay, J. Chem. Phys. **120**, 7330 (2004).
[49] R. Send and F. Furche, J. Chem. Phys. **132**, 044107 (2010).
[50] T. H. J. Dunning, J. Chem. Phys. **90**, 1007 (1989).
[51] M. J. Frisch, G. W. Trucks, H. B. Schlegel *et al.*, GAUSSIAN 09, *Revision A.1*, Gaussian Inc., Wallingford, CT, 2009.
[52] CPMD (copyright IBM Corp. 1990–2001, copyright MPI für Festkörperforschung Stuttgart, 1997–2001), http://www.cpmd.org.
[53] J. P. Perdew, K. Burke, and M. Ernzerhof, Phys. Rev. Lett. **77**, 3865 (1996).

[54] A. D. Becke, Phys. Rev. A **38**, 3098 (1988).
[55] C. Lee, W. Yang, and R. G. Parr, Phys. Rev. B **37**, 785 (1988).
[56] J. Perdew, Phys. Rev. B **33**, 8822 (1986).
[57] A. D. Becke, J. Chem. Phys. **98**, 5648 (1993).
[58] C. Adamo and V. Barone, J. Chem. Phys. **110**, 6158 (1999).
[59] N. Troullier and J. L. Martins, Phys. Rev. B **43**, 1993 (1991).
[60] H. Lischka, R. Shepard, I. Shavitt, R. M. Pitzer, M. Dallos, T. Mÿller, P. G. Szalay, F. B. Brown, R. Ahlrichs, H. J. Bšhm, *et al.*, COLUMBUS, an *ab initio* electronic structure program, release 5.9.1, 2006.
[61] I. Tavernelli, B. F. E. Curchod, and U. Rothlisberger, Phys. Rev. A **81**, 052508 (2010).
[62] M. Guglielmi, I. Tavernelli, and U. Rothlisberger, Phys. Chem. Chem. Phys. **11**, 4549 (2009).
[63] M. Barbatti, J. Pittner, M. Pederzoli, U. Werner, R. Mitric, V. Bonacic-Koutecky, and H. Lischka, Chem. Phys. **375**, 26 (2010).
[64] R. D. Mattuck, *A Guide to Feynman Diagrams in the Many-Body Problem* (McGraw-Hill, New York, 1976).
[65] I. V. Tokatly and O. Pankratov, Phys. Rev. Lett. **86**, 2078 (2001).